

Effects of pulse duration on the ns-laser pulse induced removal of thin film materials used in photovoltaics

Jim Bovatsek^{*a}, Ashwini Tamhankar^a, Raj Patel^a, Nadezhda M. Bulgakova^b, Jörn Bonse^c

^a Newport Corp., Spectra-Physics Lasers Division North America, 1335 Terra Bella Ave, Mountain View, CA 94043, USA

^b Institute of Thermophysics SB RAS, Lavrentyev ave. 1, 630090 Novosibirsk, Russia

^c Newport Spectra-Physics GmbH, Ruhlendorfer Strasse 95, 14532 Stahnsdorf, Germany

ABSTRACT

The removal of thin films widely used in photovoltaics as (transparent) electrodes (e.g. SnO₂, molybdenum) or solar absorber (e.g. amorphous silicon) materials is studied experimentally using multi-kHz diode-pumped solid state lasers in the visible and infrared spectral region. The film processing (or what is commonly known as P1, P2, or P3 laser scribing) is performed through the film-supporting glass plate of several millimeter thickness by using a galvo laser scanner setup equipped with f-theta optics. The dependence of the film removal fluence threshold on the laser pulse duration (~8 ns to ~40 ns) is investigated systematically for two different laser wavelengths of 532 nm and 1064 nm. The laser-scribing of continuous lines suitable for thin-film solar cell production is demonstrated successfully at scribe speeds on the order of meters per second. The experimental results are discussed on the basis of laser ablation models considering optical, geometrical, and thermal material properties and are additionally supported by numerical simulations.

Keywords: thin film photovoltaics, solar cell, laser scribing, P1, P2, P3, nanosecond pulse, thresholds

1. INTRODUCTION

Recent years have seen tremendous growth in emerging market economies throughout the world. The resulting rapid growth in resource consumption has driven the cost of energy to unprecedented levels. Accompanying this increased cost was increased interest in alternative energy sources such as photovoltaic (“PV”) devices. And with every surge in the price of oil or gas, there was a corresponding surge in the financial viability of such alternatives. While recently the rate of global economic growth has waned, and the cost of energy has retreated accordingly, interest in solar cell technology remains strong. This is providing a source of continued demand for various support industries such as laser and laser-based system manufacturing.

The role of lasers in solar cell device fabrication continues to expand, with processes such as cutting, drilling, scribing, sintering, and annealing all being explored. For the highly-efficient crystalline silicon-based devices (“c-Si”), lasers are most commonly used for edge isolation scribing; but there is also a fast-growing application space with the increased fabrication of more exotic solar cells, such as “emitter wrap through” (via drilling) and buried contact (scribing) devices.¹

An increasingly popular alternative to c-Si solar cells is thin film photovoltaic (TFPV) device technology, for which the most important laser process is laser thin film removal (“laser scribing”) for electrical isolation of the individual segments of a monolithically integrated serial connection of solar cells. This process involves the irradiation of a glass panel with a tightly-focused laser beam, thus resulting in the removal of one or more layers of thin film from

either another thin film material, or from the glass panel itself. In the production of a thin film solar cell device, three scribes processes are typically performed (commonly referred to as the P1, P2, and P3 scribes), with various film deposition processes occurring in between. The P1 scribe removes a first electrical contact film from the glass substrate; the P2 scribe removes the solar absorber film from this first contact film; and the P3 scribe removes both the PV layer and a second electrical contact film from the first contact film.

This study focuses on laser thin film scribe processes for various thin film solar technologies including amorphous Silicon (P1, P2, P3 scribes), CdS/CdTe (P1 scribe only) and CIGS (P1 scribe only). The energy density (also known as fluence) threshold for removal of the thin film(s) of interest is determined for various pulse durations between approximately 10 and 40 nanoseconds, and for IR (1064 nm) and green (532 nm) wavelengths. For selected scribe processes, experimental results are compared to those generated by a thermal model of the laser irradiation process.

1.1 Thin film photovoltaic devices

The monolithic thin film solar cell is increasingly the architecture of choice for solar cell manufacturing companies worldwide. There are several reasons for this, including attractive manufacturing scalability, opportunities for leveraging existing flat panel display technology, and the potential shortage of bulk silicon used for more efficient crystalline Silicon (“c-Si”) solar cells. In addition, various process- and materials-related technology advancements are improving device efficiencies, resulting in an increasingly attractive balance between manufacturing cost and product performance.²

Varieties of thin film solar cells include amorphous Silicon (“a-Si”), Cadmium Sulfide/Cadmium Telluride (“CdS/CdTe”), and Copper Indium Gallium di-Selenide (“CIGS”); substrates for cell fabrication include several-millimeter thick soda lime glass as well as polymers and metals with thicknesses in the range of 10’s of microns.

While the materials involved are varied, each with particular advantages and disadvantages, all thin film solar cells share the same basic geometry and working principle. Figure 1 shows a cross-sectional schematic of such a typical thin film photovoltaic device. The materials are arranged in a layered system such that there are two electrically-conducting “contact” surfaces (“front-side“ (facing the sun) and “back-side” contacts) with a semiconductor (PV) material as solar absorber in between. Front-side electrical contacts utilize TCO (transparent conducting oxide) materials, such as ITO or SnO₂, which allow both sunlight and electricity to propagate within them with minimal loss.

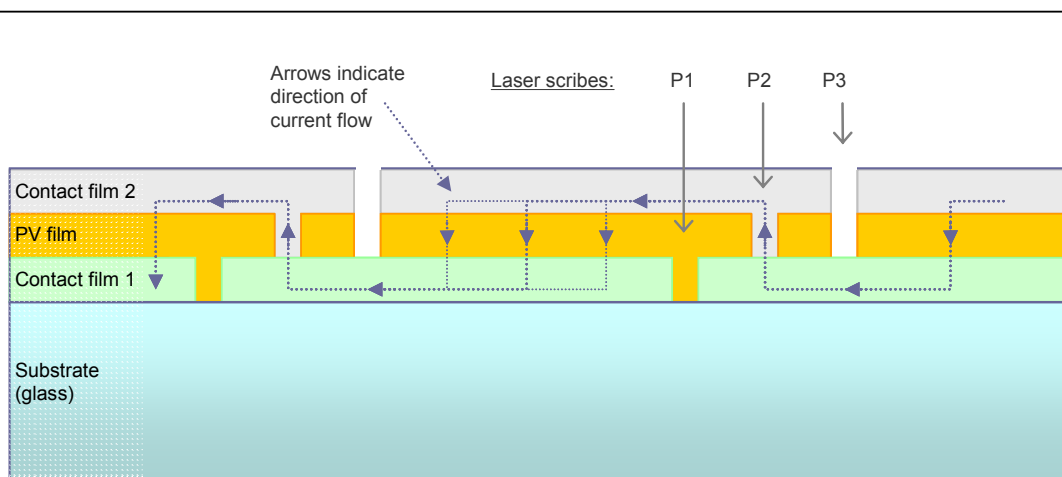


Figure 1. Schematic showing the basic geometry and functioning of a thin film solar cell.

The laser scribes are identified as “P1”, “P2”, and “P3” and their purpose is to divide the large, meter-sized solar panels into several narrow PV cells operating electrically in series. This results in a more practical and efficient low-current/high-voltage device.

1.2 Thin film scribing with q-switched lasers

Various types of lasers are employed for thin film scribing, with diode-pumped solid state (“DPSS”) q-switched lasers, at both infrared and green wavelengths, among the most common. Short pulse widths in the range of 10’s of nanoseconds combined with 10’s of microJoule pulse energy levels provide sufficient intensity for most film removal tasks. To meet the throughput demands of high-volume manufacturing, relative motion between the glass panel and the irradiating laser beam (achieved either by beam scanning, or panel motion) is minimally several hundred mm/s, and up to several m/s in the most advanced systems. To keep up with the high-speed motion, the lasers must be capable of generation pulses at a rate of 10’s to 100’s of kHz.

When possible, it is generally preferred to scribe with the laser incident from the substrate-side of the target film(s). For example, if the goal is to remove an absorbing metal film from a transparent glass substrate, the laser pulses will ideally travel through the glass before irradiating the metal/glass interface. Figure 2 illustrates such a scenario, and indicates the various physical phenomena (ablation, delamination, etc.) that are potential contributors to the film removal process.

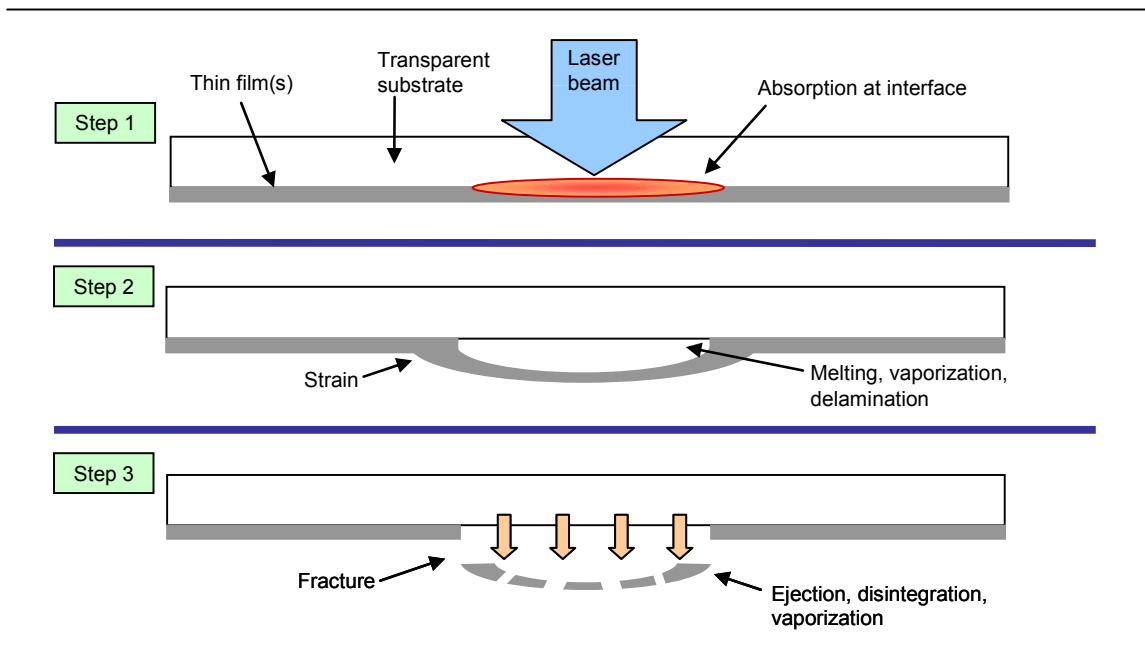


Figure 2. Illustration depicting thin film removal with laser incidence through the transparent substrate.

Generally, the thin film removal process with ns-pulse irradiation may be considered to occur in three steps (Fig. 2). During the first step, the optical laser pulse energy is absorbed at the film/glass interface leading to step temperature increase. During the second step, this temperature increase leads to local thermal strain and eventually to melting and evaporation. If fracture or sufficient evaporation occurs, the film may disintegrate and ablate in the subsequent third process step.

Compared to film-side irradiation, this method can lead to more efficient scribing through a reduction in fluence threshold for laser damage and/or the ability to remove the entire film with single- vs. multi-pulse processing. Additional potential benefits include less debris formation/deposition, and less plasma/debris shielding of the laser

pulses. Care must be taken to avoid excessive optical absorption by the substrate of the irradiating wavelength, leading to substrate damage; however for the common case of a (transparent) glass substrate and IR or green laser wavelength, this is generally not a concern since the threshold for film removal is typically lower than that for damaging the glass.

2. EXPERIMENTAL DETAILS

In this study, four different laser systems were used to execute four unique scribe processes, including two P1 scribes and the a-Si P2 and P3 scribes. For each of the processes, film removal thresholds were determined for 532-nm irradiation wavelength at three unique pulse durations between about ~8 ns and 40 ns. In addition, P1 scribe thresholds were determined for 1064-nm irradiation wavelength and sub-10ns pulses. The scribed thin film materials include Molybdenum, SnO₂, a-Si, and a film stack composed of a-Si+ZnO+Al. The base substrate material for all film stacks is ~3-mm thick soda lime glass; however the a-Si and a-Si/ZnO/Al layers are deposited on top of a SnO₂ film (which is ideally undamaged by the laser scribe process). Scribe threshold values were determined by correlating variations in applied pulse energy with the size of the resulting film removal areas.

2.1 Laser systems

Four Newport/Spectra-Physics diode pumped solid state q-switched laser systems were used to generate data presented here: Explorer® 532- and 1064-nm system, BL6S 532-nm laser system, and Navigator II 532-nm laser system. A listing of the operating parameters for the lasers can be found in Table 1. In combination, this group of lasers is capable of generating a range of power levels (~1 – 10 W) and pulse durations (~6-70 ns), with the capability of both infrared (1064 nm) and green (532 nm) output wavelengths. Furthermore, the four systems have TEM₀₀ mode output with $M^2 < 1.3$. For the threshold tests, the lasers were used to generate pulse durations in the range of 8 ns (Explorer™) to 37 ns (Navigator II).

Table 1. Performance specifications of lasers used in the tests.

Laser system	Wavelength [nm]	Av. Power [W]	PRF, range [kHz]	Pulse width [ns]
Explorer®-532	532	>1	20 – 150	~6-18
Explorer®-1064	1064	>1.75	20 – 150	~6-18
BL6S-532	532	>2.7	10 – 60	~7-14
Navigator™ II	532	>9	15 – 100	35-70

In Table 1, the quoted power levels are typical maximum. For the BL6S™ and Navigator II laser systems, the output power at 532 nm changes significantly with the pulse repetition frequency (PRF) because the harmonic conversion efficiency changes with changes in pulse energy (high PRF = low pulse energy, and vice-versa). Conversely, the Explore®-532 laser system uses intra-cavity harmonic conversion, which allows for a more constant output power through a wide range of repetition rates. Also note that the pulse durations are specified as a range of values. Larger values are achieved by operating the laser at a higher PRF, and smaller values are achieved with lower PRF.

2.2 Optical set-up

The optical set-up used for the tests consists of four steering mirrors directing the laser pulses into a galvanometer-based beam scanning system (“galvo scanner”) with 10-mm diameter input aperture. Two different f-theta lenses with focal lengths of 80 and 160 mm were used for all beam focusing. When necessary, beam-collimating and/or beam-expanding optics were implemented to help generate the desired optical spot sizes. All threshold data was generated with focused $1/e^2$ -beam diameters in the range of 30-55 μm (verified experimentally).

2.3 Threshold determination

When discussing a material's "damage" or "ablation" threshold, it is important to clarify precisely what phenomenon the threshold is for. In many cases, a laser damage threshold is simply the energy density (in J/cm^2) which causes a visible surface modification of the material; alternatively, the threshold of interest may be that fluence which results in crater formation in the material. For identical materials, we would likely find a large discrepancy in threshold values for (i) slight visible surface modification and (ii) measureable removal of bulk material.

In the case of laser thin film photovoltaic scribing, we are interested in *complete removal of the film* to the extent that is detectable with optical microscopy and/or surface profilometry (in practice, the true success of a PV scribe is defined by the final photo-electrical performance of the finished solar cell; however, experience has shown that visual inspection is usually a sufficient predictor of performance). And so the thresholds presented here represent the fluence that will result in the complete removal of the particular film(s) of interest from the immediate underlying material (substrate).

One very straightforward method to determine the threshold fluence for laser-induced bulk material modification has been described first in 1982 by J.M. Liu³, which has been later adopted for application to thin film removal by several other researchers.⁴⁻⁶ The method involves generating single-pulse laser damage features at different pulse energies (but the same focus spot size), measuring the diameters of the features, and using log-linear regression techniques to infer the relevant threshold fluence. This technique is attractive because in addition to the threshold information, it also allows for precise experimental determination of the optical spot size that was used to generate the features. This number can then be compared to a calculation based Gaussian beam propagation theory to further validate the threshold results. We estimate the accuracy of the thresholds derived with this method at $\pm 20\%$.

2.4 Materials

Removal thresholds were determined for single-layer thin films of SnO_2 (a-Si and CdS/CdTe devices, P1 scribe), Molybdenum (CIGS device, P1 scribe), amorphous Silicon (a-Si device, P2 scribe), and a multilayer stack of a-Si+ZnO+Aluminum (a-Si device, P3 scribe). The film thicknesses of the materials along with relevant experimental parameters are listed in Table 2. For SnO_2 and Molybdenum, the threshold is for complete film removal from a glass substrate; for the a-Si P2 and P3 scribes, the threshold is for complete removal from a sub-micron thick layer of SnO_2 film on glass.

These materials are used extensively in the thin film photovoltaic industry; and scribe processes involving them are required in the manufacturing of a-Si, CdS/CdTe, and CIGS type devices.

3. RESULTS AND DISCUSSION

The removal threshold values determined for the various pulse durations, wavelengths, and scribe processes are listed in Table 2. The data shows a wide range of removal thresholds amongst the various materials, from ~ 0.1 to $>2.0 \text{ J}/\text{cm}^2$ (20:1 variation in fluence). The table also shows the approximate $1/e^2$ -spot size (diameter) that was extracted from the threshold-determination data.

Table 2. Film removal thresholds for different pulse durations and wavelengths.

Scribe type	TFPV Type	Film(s)/substrate	Film / substrate thickness [μm]	Wave-length [nm]	Pulse width [ns]	Optical spot size, $1/e^2$ [μm]	Fluence threshold [J/cm^2]
P1	a-Si, CdS/CdTE	SnO ₂ / glass	0.650 / 3000	532 532 532	9 13 37	33 43 38	1.43 1.03 2.04
P1	a-Si, CdS/CdTE	SnO ₂ / glass	0.650 / 3000	1064	7	44	2.19
P1	CIGS	Moly / glass	0.293 / 3000	532 532 532	9 13 37	36 54 37	1.22 1.21 1.07
P1	CIGS	Moly / glass	0.293 / 3000	1064	7	39	1.01
P2	a-Si	a-Si / SnO ₂	0.220 / 0.650	532 532 532	13 17 37	51 32 40	0.115 0.182 0.194
P3	a-si	Al+ZnO+a-Si / SnO ₂	0.570 / 0.650	532 532 532	13 17 37	51 33 43	0.110 0.181 0.247

With knowledge of the film removal thresholds, it is then possible to optimize the laser parameters and generate continuous scribes of removed material, exactly as required in the manufacture of the solar cell devices. Figure 3 below shows microscope photos of such scribes for the materials that were studied, using the focused beam sizes listed in Table 2. This data demonstrates that the chosen laser sources are suitable for thin-film solar cell production at scan speeds on the order of m/s, even at relatively low power levels (i.e. <1W).

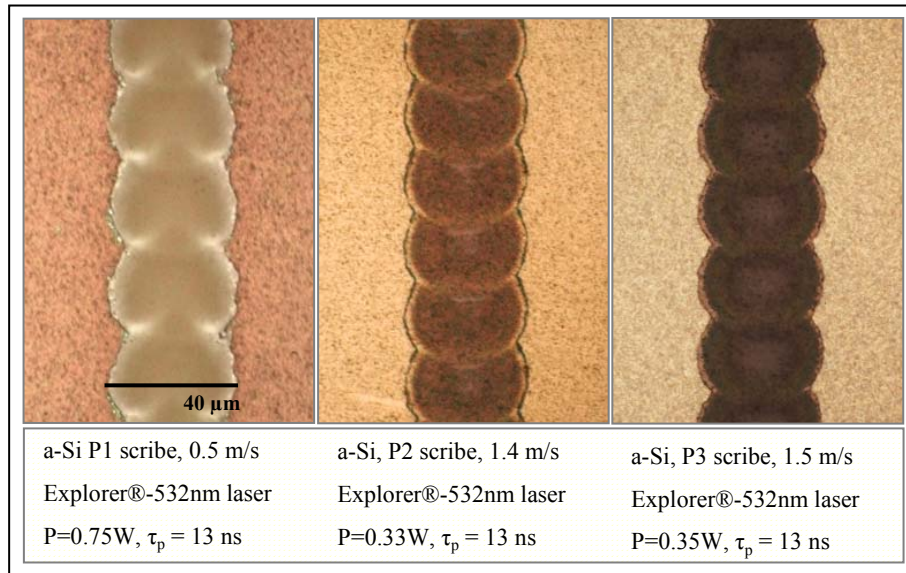


Figure 3. Microscope photos of P1, P2, and P3 a-Si thin film photovoltaic device scribes generated using threshold data from this study.

3.1 P1 scribe thresholds: SnO₂ and Molybdenum

For the P1 materials, threshold-dependence on pulse duration is not very definitive, with film removal thresholds at increasing pulse widths trending somewhat higher for SnO₂, and somewhat lower for Molybdenum. Based solely on thermal diffusion arguments, we might expect that, for longer pulse durations, the threshold would increase in proportion to the square root of the ratio of the pulse durations.⁷ However, for the case of thin films with thicknesses similar or below the spatial thermal diffusion during the laser pulse irradiation time, it is not very surprising to see a breakdown in this relationship.

3.2 P2 and P3 scribe thresholds: amorphous Silicon

The a-Si P2 and P3 scribe threshold results are of particular interest. Very little energy density is required for complete removal of the film. Clearly, the strong absorption of silicon at 532 nm is assisting the film removal process. There is also a significant pulse-width dependence compared to the P1 scribe results. For a pulse duration change from 13 ns to 37 ns (2.85×), there is a threshold change of 0.115 to 0.194 J/cm² (1.68×) for the P2 scribe and 0.110 to 0.247 J/cm² (2.25×) for the P3 scribes. This result, which is visualized in the following Figure 4, indicates that a clear processing advantage exists with, for example, ~10 ns vs. ~40 ns pulse durations, potentially allowing for 50% percent improvement in processing efficiency.

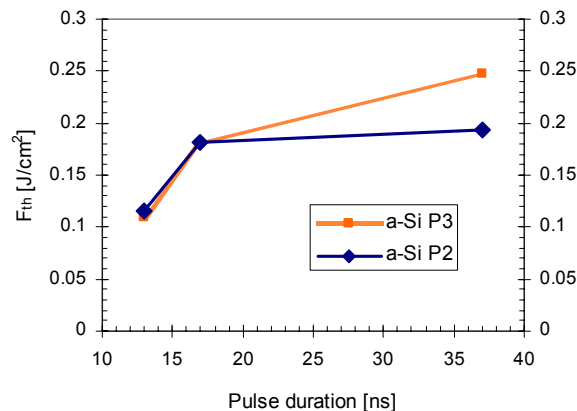


Figure 4. Illustration depicting thin film removal with laser incidence through the transparent substrate.

In addition to the strong threshold dependence on pulse width, the a-Si P2/P3 threshold results are also interesting for their very low absolute fluence levels, irrespective of the irradiating pulse width. At the 532-nm wavelength, the regime of 0.1 – 0.2 J/cm² for the complete removal of the a-Si films is significantly below damage threshold values reported for bulk crystalline silicon, where, at a comparable laser pulse duration of 18 ns, laser-induced melting has been observed for fluences larger than 0.35 J/cm² (see Ref. 8). This cannot be explained solely by differences in the optical properties. Such a discrepancy indicates a different material removal mechanism and justifies a more detailed theoretical physical analysis.

3.3 Thermal modeling and analysis

For the a-Si P2 and P3 scribes, a thermal model for the pulsed irradiation of the samples was applied. The output of the numerical analysis is the one-dimensional temperature vs. time distribution in the various layers of the film stack. Thermal modeling was recently performed for films on a substrate (metal on metal,⁹ metal on glass,^{10,11} and polymer on glass,¹²) irradiated with fs and ns laser pulses. To our knowledge, the application of such model to the case of a multiple thin film photovoltaic layer stack (including P2 and P3) is the first of its kind. The multilayer structures of interest are presented schematically in Figure 5 as “sample 2” and “sample 4”.

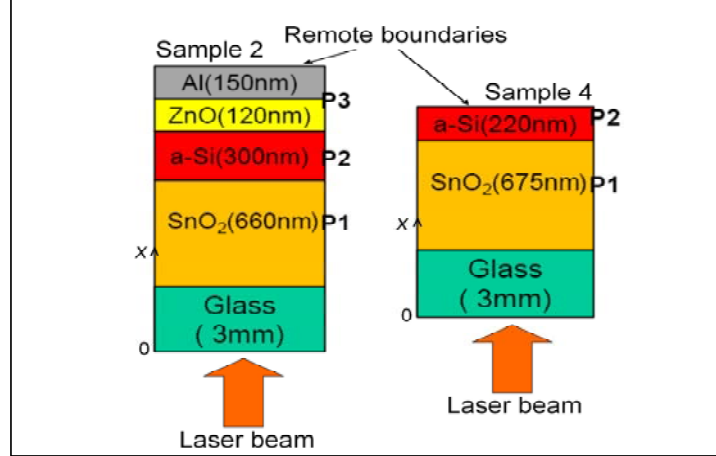


Figure 5. Illustration depicting thin film removal with laser incidence through the transparent substrate.

Details of the thermal model are described in Ref. 13. Here we explain only its main features. The time-dependent temperature distribution in the irradiated sample $T(t,x)$ is governed by the heat flow equation in a one-dimensional form:

$$\left(c_p \rho + L_m \delta(T - T_m)\right) \frac{\partial T}{\partial t} = \frac{\partial}{\partial x} \lambda \frac{\partial T}{\partial x} + \Sigma(x,t). \quad (1)$$

Here, ρ is the mass density of the target material; c_p and λ are the thermal capacity and the thermal conductivity of the target material, respectively. The term $\Sigma(x,t)$ represents the spatio-temporal source of the laser energy which will be defined below.

The term $L_m \delta(T - T_m)$ (L_m is the latent heat of fusion) is introduced for a case of melting of the irradiated sample. This term allows performing the through calculations of the liquid–solid interface whose temperature is assumed to be continuous and equal to T_m .

Note that in the formulation of the Eq. (1) thermal vaporization is disregarded in view of relatively low laser fluences which are insufficient for heating of the considered materials above the melting threshold and, thus, to initiate thermal vaporization.

Equation (1) is calculated for each layer of a particular structure (Fig. 5) while taking into account the physical properties of a material composing the layer (see Tables 3). Initially, the sample is assumed to be at room temperature (300 K). The glass substrate is considered to be completely transparent. The laser pulse couples the SnO_2 -layer from the side of the glass substrate so that the laser energy source in the SnO_2 layer is written as

$$\Sigma(x,t) = (1 - R_{\text{FU}})(1 - R_{\text{P1}})\alpha_{\text{P1}}I(t) \exp(-\alpha_{\text{P1}}(x - \Delta X_{\text{FS}})). \quad (2)$$

Here $I(t)$ is the incident laser pulse intensity with the Gaussian temporal shape, α_{P1} and R_{P1} are the absorption and reflection coefficients of SnO_2 , and x is the distance calculated from bottom of the calculational region (see Fig. 5). ΔX_{FS} is the thickness of the glass substrate, which is limited here to $2\mu\text{m}$ (this was found to be sufficiently large for modeling of the thermal penetration during the time of interest). For the absorbing P2 layer, the laser energy source is constructed in the following form:

$$\Sigma(x,t) = (1 - R_{\text{FU}})(1 - R_{\text{P1}})(1 - R_{\text{P2}})\alpha_{\text{P2}}I(t) \exp(-\alpha_{\text{P2}}(x - \Delta X_{\text{FS}} - \Delta X_{\text{P1}})) \exp(-\alpha_{\text{P1}}\Delta X_{\text{P1}}), \quad (3)$$

where ΔX_{p1} is the thickness of the SnO₂ layer. The laser energy source terms are constructed similarly for the ZnO and Al layers of the sample 2. However, it should be noted that, in view of relatively large thickness of the absorber, only a negligible portion of the laser energy reaches the P3 layer. The model provides also for the change in optical properties of P2 layer upon melting via reconstructing the term (3) into molten and solid layers. However, for the irradiation regimes considered here, the melting temperature is not reached.

The boundary conditions at the interfaces between the layers provide for free heat flow that can be expressed in the following form

$$\lambda_{FS} \frac{\partial T}{\partial x} \Big|_{FS} = \lambda_{P1} \frac{\partial T}{\partial x} \Big|_{P1}, \quad \lambda_{P1} \frac{\partial T}{\partial x} \Big|_{P1} = \lambda_{P2} \frac{\partial T}{\partial x} \Big|_{P2}, \quad \text{etc.} \quad (4)$$

At the bottom boundary $x = 0$ (Fig. 5), the temperature was considered to be 300 K and, at the upper remote boundary from the laser, the condition of the absence of heat flow through the surface was applied as $\frac{\partial T}{\partial x} = 0$. This

condition implies the absence of vaporization in view of the relatively low applied laser fluences which, as will be demonstrated below, are too low to initiate melt and vaporization of the material. In the nanosecond time scale, we also disregard cooling of the surface by an ambient gas as well as radiative cooling.

The thermal problem (the differential equation including its boundary conditions) has been solved in only a one-dimensional approach, which is justified in view of the large irradiation spot size and comparatively shallow thermally-affected depth over the computational time. We have used an explicit numerical scheme with a spatial step of 2.5 nm and a time step of 20 ps which secure numerical scheme stability and good approximation of the solved differential equation.

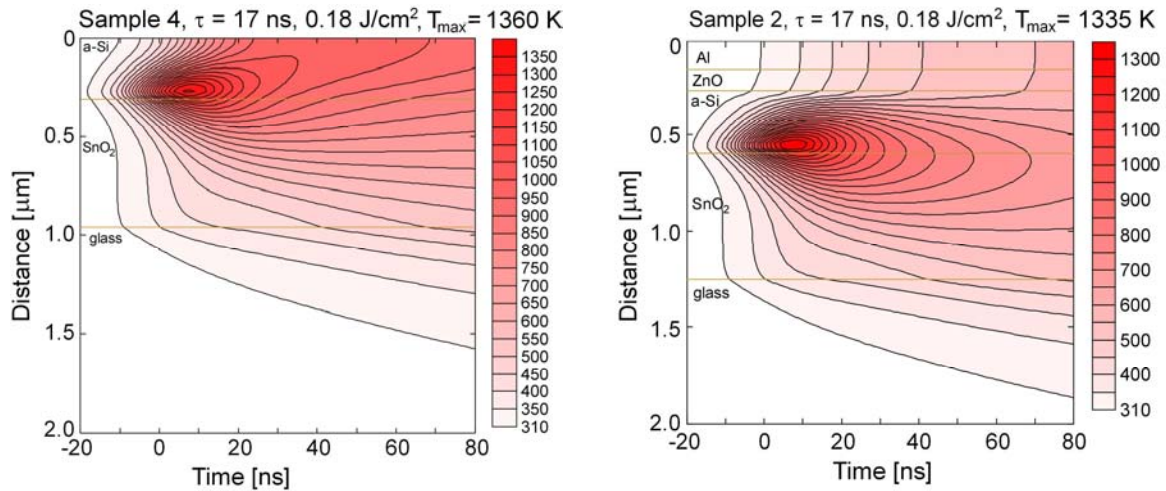


Figure 6. Spatio-temporal behavior of the temperature in the a-Si P2 (left) and P3 (right) samples under irradiation of laser pulses (17 ns duration, 532 nm wavelength). The laser fluence of 0.18 J/cm² corresponds to the experimentally determined scribing threshold value. Note that distance here is counted from the remote boundary, contrary to Fig. 5.

Figure 6 shows the results of the numerical integration of the thermal problem [Eqns. (1)-(5)] for ns-laser pulse irradiation (17 ns, 532 nm) of the two multi-layer systems of interest (sample 2 and sample 4 for the P2 and the P3 scribes, respectively) at the experimentally determined threshold value for complete a-Si film removal (0.18 J/cm²). The spatio-temporal behavior indicates that the maximum temperature of ~1350 K is reached immediately after the laser pulse (the intensity maximum of the laser pulse is chosen at the time $t = 0$), before heat diffusion along the

layers redistributes the absorbed laser pulse energy and cools down the irradiated spot. Interestingly, the maximum temperature reached is very similar for both samples, which indicates that the additional Al/ZnO overlayers do not significantly affect the heat flow and the film removal thresholds. Moreover, the maximum temperature value of ~1350 K is below the melting (1420 K) and boiling (2654 K) temperatures of the (amorphous) silicon material.⁷ This observation directly proves that the thermal mechanism of melting and subsequent evaporation are not responsible for the a-Si film removal during the laser scribing process here.

Table 3. Material properties used in thermal modeling.

Parameter	Material	Value	Ref.
Density ρ , [g/cm ³]	a-Si	2.2	14
	l-Si	2.52	14
	glass	2.2	14
	Al	2.69	15
	SnO ₂	6.95	15
	ZnO	5.7	15
Melting temperature, T_m , [K]	a-Si	1420	7,14
	Glass (softening)	1956	16
	Al	933	15
	SnO ₂	1898	15
	ZnO	2248	15
Latent heat of fusion, L_m , [J/kg]	a-Si	1.32×10^6	14
	Al	4×10^5	15
	SnO ₂	3.17×10^5	15
	ZnO	9.7×10^5	7
Specific heat, c_p , [J/(kg·K)]	c-Si	$184.36 \times \exp(4.5 \times 10^{-3}T)$, $T < 300$ K	14
		$695.54 \times \exp(2.375 \times 10^{-4}T)$, $T \geq 300$ K	
	a-Si	$C_p(\text{c-Si}) - 8.0029 + 0.1017T$	14
		800	7
	l-Si	910	7,14
	glass	$708.11 + 0.29917 \times T$	14
	Al	901	15
	SnO ₂	353	15
	ZnO	494	15
Thermal conductivity, λ , [W/(m·K)]	a-Si	1.8	14
	l-Si	$50.28 + 0.02933 \times (T - T_m)$	14
	Glass	$1.0056 + 1.3 \times 10^{-3}T$, $T \leq 1170$ K	14
		2.514, $T > 1170$ K	
	Al	240, $T \leq 400$ K	17
		$240 - 0.05(T - 400)$, $400 \text{ K} < T < T_m$	
		93, $T \geq T_m$	
	SnO ₂	3.2	7
ZnO	29		
Refractive index $n+ik$ @ 532 nm	a-Si	$4.49 + i0.97$	18
	l-Si	$3.00 + i4.80$	19
	Glass	1.50	20
	Al	$0.88 + i6.48$	20
	SnO ₂	$1.89 + 0.01$	20
	ZnO	2.03	20

3.4 Thermal stress analysis

Since the threshold fluences of the a-Si P2/P3 scribes are found to be somewhat lower than what is required to initiate melting of the silicon, it is useful to further explore the problem. In particular, the effects of rapid thermal expansion due to the rapid heating via short-pulse laser irradiation should be considered.

To evaluate stress components generated in the a-Si film under fast heating, the approximate solution of the thermo-elasticity problem for a round plate with fixed edges may be used:¹⁰

$$\sigma_{r \max} = \sigma_{\theta \max} = \frac{E \alpha_l \Delta T}{2(1-\nu)} \quad , \quad (5)$$

where E is the Young's modulus, α_l is the coefficient of linear thermal expansion, ν is the Poisson ratio, and ΔT is the temperature difference along the radius. For evaluation, we use the following mechanical properties of amorphous silicon: $E = 80 \text{ GPa}$,²¹ $\nu = 0.22$,²¹ $\alpha_l \approx 4 \times 10^{-6} \text{ K}^{-1}$.²² For the samples 2 and 4, the simulations have given the values ΔT in the range of 700 – 1000 K. This results in stress values within the a-Si layer in the range 150 – 200 MPa. These values are much higher than the expected yield stress, which is below 10 MPa at $T \geq 700 \text{ K}$ for crystalline silicon.²³ The tensile strength, which is of order of few GPa for single- and polycrystalline silicon,^{24,25} is much lower for amorphous silicon.²⁵ Hence, the irradiated area of the sample 4 experiences plastic deformations and can be fractured under laser-induced thermal stresses at the temperatures well below the melting point.

With regard to the P3 scribe process (sample 2, Fig. 6), the presence of the Al/ZnO layers atop the a-Si film may be considered to have two effects: (i) increased resistance to the fracturing of the a-Si layer, and (ii) partial heat extraction due to high thermal conductivity. However, note that the threshold laser fluence at 17 ns pulse duration is very similar for the Samples 2 and 4, see Table 2. Furthermore, it is apparent that, while the Al/ZnO layer does in fact change the spatio-temporal temperature distribution within the a-Si film, it does not reduce considerably the maximum temperature reached in the layer. Hence, the rapid thermal expansion and associated thermal stress in the absorbing a-Si layer is similar for both samples.

Considering the mechanical aspects of the presence of the Al/ZnO films, we find that the tensile strength of ZnO films is reported to be quite high, on the order of 400 MPa²⁶ (for pure aluminum it is only 90 MPa²⁷). We note, however, that tensile stress is usually reported for quasi-static loading. Dynamic loading of the nanosized Al/ZnO film on the nanosecond timescale, when the underlying heated silicon film expands abruptly, may in fact lead to failure of the brittle P3 film material, with the occurrence of crack formation and subsequent disintegration.²⁸

An additional, practical consideration relates to the Gaussian intensity distribution of the irradiating laser beam. When a single laser pulse removes a region of thin film, the outer periphery of this region demarcates where the irradiating energy density was precisely equal to the film removal threshold. Closer towards the center of the feature, the material is exposed to increasingly higher intensities. Depending on the pulse energy and beam focus spot size, this difference in fluence can be quite high; and in the context of P3 film removal, this central fluence may in fact be high enough to generate thermal strain beyond the tensile strength of ZnO. This analysis implies that there is a certain threshold fluence beyond which both the a-Si and the Al/ZnO film are removed; and below which the a-Si film is damaged, but the mechanical strength of the ZnO film prevents complete blow-off of the layers. This scenario is illustrated in Figure 7, which contains microscope photos of features used to determine the film removal threshold for 532-nm wavelength and 13-ns pulse duration with optical beam spot size of 51 μm ($1/e^2$).

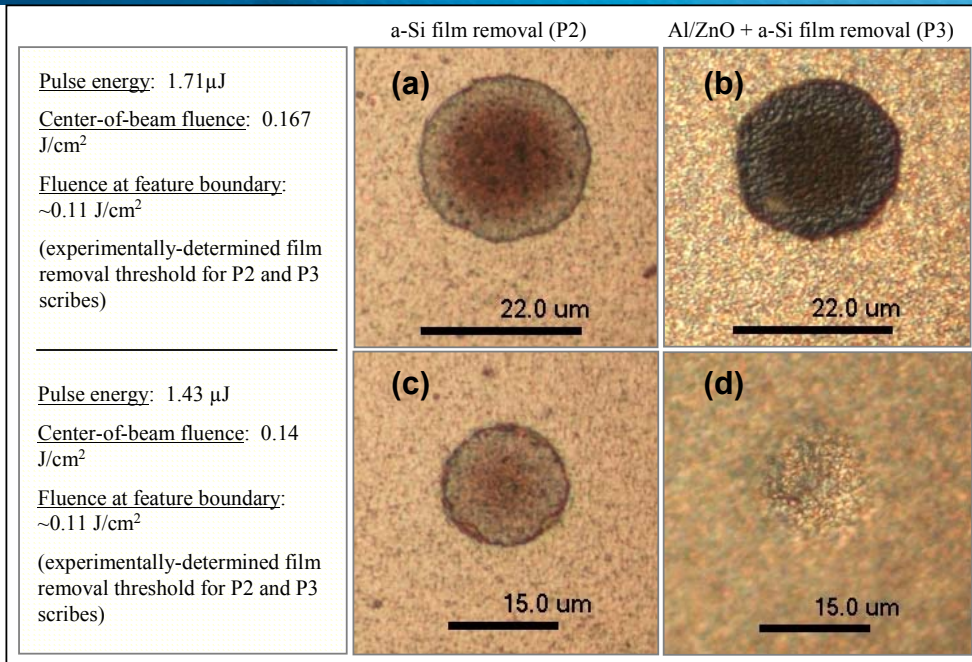


Figure 7. Microscope photos of P2 and P3 film removal features using 532-nm, 13-ns pulses. For the lower pulse energy of 1.43 μ J, the mechanical strength of the ZnO film is sufficient to prevent complete film removal (picture at bottom-right).

The photos in Figure 7 indicate that the 1.71- μ J laser pulse energy is sufficient for generation of 22- μ m wide features for both P2 and P3 film removal processes [Figs. 7(a) and (b)]. However, the reduced pulse energy of 1.43 μ J is sufficient only for removal of the a-Si film [Fig. 7(c)]. With the additional Al/ZnO film stack, the lower pulse energy results in only a bulging of the film, and a very slight fracture of the film at the center of the irradiation area, for the lower pulse energy [Fig. 7(d)].

4. CONCLUSIONS

Threshold-dependence on pulsed duration (8 ns – 40 ns) for various thin film photovoltaic scribe processes (P1, P2, P3) has been characterized, with selected scribes also being tested for wavelength dependence (1064 nm vs. 532 nm). For SnO₂ and Molybdenum P1 scribing, there is no clear trending of film removal threshold with pulse duration; likewise, there is no clear advantage of using 532-nm over 1064-nm wavelength, or vice versa, in terms of the expected processing efficiency. However, threshold-dependence on pulse duration was clearly demonstrated for the a-Si P2 and P3 scribes with the 532-nm wavelength, with a noteworthy advantage for shorter pulses. Compared to 40-ns pulses, 10-ns pulses can process these films at ~50% lower energy densities, thus allowing for increased processing efficiency, reduced thermal loading of the substrate, and lower overall manufacturing costs for thin film photovoltaic devices.

For all pulse durations at the 532-nm wavelength, the film removal thresholds for a-Si P2 and P3 processes were found to be very low (0.1 – 0.25 J/cm²). Thermal modeling of the pulsed irradiation process indicates that these fluence levels are too low to initiate melting of the silicon. However, additional thermo-mechanical analysis has shown that the thermal strain induced by rapid thermal expansion of the silicon is well beyond the material's yield strength, and is therefore likely responsible for fracture and delamination of the silicon (and additional layers atop it).

Our results demonstrate that, while no clear advantage exists for short pulse P1 scribe processes, there is a significant advantage for the a-Si P2 and P3 scribe processes. Within the range of pulse durations and wavelengths

we have studied, execution of the three primary thin film photovoltaic scribe processes is easily achieved at the m/s level with the use of advanced q-switched diode pumped solid-state lasers available in the market today.

ACKNOWLEDGMENTS

We would like to extend special thanks to Nadezhda Bulgakova of the Institute of Thermophysics in Novosibirsk, Russia, for the excellent theoretical analysis of the various physical phenomena. In addition to the work presented here, she has provided many thoughtful comments and discussions for which the authors are grateful. The authors would also like to thank Gonzalo Guadano for his efforts in supporting this work; his technical expertise is greatly appreciated.

REFERENCES

- [1] Mingirulli, N., Trittler, S., Bui, M., Grohe, A., Biro, D., Preu, R., Glunz, S., 23rd EPVSEC, Valencia, Spain (2008).
- [2] Patel, R., Clark, D., Bovatsek, J., Proc. ICALEO 2007, Orlando (2007).
- [3] Liu, J. M., Opt. Lett. 7, 196-198 (1982).
- [4] Jandeleit, J., Urbasch, G., Hoffmann, H. D., Treusch, H.-G., and Kreutz, E. W., Appl. Phys. A 63, 117-123 (1996).
- [5] Bonse, J., Baudach, S., Kautek, W., Welsch, E., and Krüger, J., Thin Solid Films 408, 297-301 (2002).
- [6] Choi, H.W., Farson, D. F., Bovatsek, J., Arai, A., and Ashkenasi, D., Appl. Opt. 46, 5792-5798 (2007).
- [7] Bäuerle, D. [Laser Processing and Chemistry], 3rd edition, Springer-Verlag, Berlin, (2000).
- [8] Lowndes, D. H., Wood, R. F., and Westbrook, R. D., Appl. Phys. Lett. 43, 258-260 (1983).
- [9] Melnikov, A., Prima-Garcia, H., Lisowski, M., et al., Phys. Rev. Lett. 100, 107202 (2008).
- [10] Meshcheryakov Y. P., and Bulgakova, N. M., Appl. Phys. A 82, 363-368 (2006).
- [11] Hermann, J., Benfarah, M., Bruneau, S., et al., J. Phys. D 39, 453-460 (2006).
- [12] Fardel, R., Nagel, M., Lippert, T., et al., Appl. Phys. A 90, 661-667 (2008).
- [13] Bulgakova, N. M., Bulgakov, A. V., and Babich, L. P., Appl. Phys. A 79, 1323-1326 (2004).
- [14] De Unamuno, S., and Fogarassy, E., Appl. Surf. Sci. 36, 1-11 (1989).
- [15] Grigoryev, I.S., Meilikhov, and E.Z., Radzig, A.A. (Eds.) [Handbook of Physical Quantities], CRC Press, (1995).
- [16] Website, <http://www.camglassblowing.co.uk/gproperties.htm>
- [17] Approximated on the basis of the temperature dependent data from Samsonov, G.V. (Ed.), [Physicochemical Properties of the Elements], Naukova Dumka, Kiev, (1965). (in Russian)
- [18] Palik, E.D. (Ed.), [Handbook of Optical Constants of Solids], Academic Press, Orlando FL, (1998).
- [19] Fuchs, M.S.K., J. Phys.: Condens. Matter 12, 4341-4351 (2000).
- [20] Website, <http://www.luxpop.com>
- [21] Freund, L.B., and Suresh, S., [Thin film materials], Cambridge University Press, (2003).
- [22] Fabian, J., and Allen, P. B., Phys. Rev. Lett. 79, 1885-1888 (1997).
- [23] Rabier, J., and Demenet, J. L., Phys. Stat. Sol. (b) 222, 63-74 (2000).
- [24] Tsuchiya, T., Hirata, M., Chiba, N., et al., J. Microelectromechanical Systems 14, 1178-1186 (2005).
- [25] Tsuchiya, T., 13th Int. Conf. Solid State Sensors, Actuators, and Microsystems 2, 1953-1956 (2005).
- [26] Ong, C. W., Zong, D. G., Aravind, M., Choy, C. L., and Lu, D. R., J. Mater. Res. 18, 2464-2472 (2003).
- [27] <http://www.azom.com/details.asp?ArticleID=2538>.
- [28] Zhou, F., and Molinari, J.-F., Comput. Methods Appl. Mech. Engin. 194, 1693-1709 (2005).